Explicit Directivity-Pulse Inclusion in Probabilistic Seismic Hazard Analysis

Polsak Tothong,[a] M.EERI, C. Allin Cornell,[b] M.EERI, and J. W. Baker,[c] M.EERI

Probabilistic seismic hazard analysis (PSHA) is widely used to estimate the ground motion intensity that should be considered when assessing a structure's performance. Disaggregation of PSHA is often used to identify representative ground motions in terms of magnitude and distance for structural analysis. Forward directivity–induced velocity pulses, which may occur in near-fault (or near-source) motions, are known to cause relatively severe elastic and inelastic response in structures of certain periods. Here, the principles of PSHA are extended to incorporate the possible occurrence of a velocity pulse in a near-fault ground motion. For each magnitude and site-source geometry, the probability of occurrence of a pulse is considered along with the probability distribution of the pulse period given that a pulse does occur. A near-source "narrowband" attenuation law modification to predict ground motion spectral acceleration (S_a) amplitude that takes advantage of this additional pulse period information is utilized. Further, disaggregation results provide the probability that a given level of ground motion intensity is caused by a pulse-like ground motion, as well as the conditional probability distribution of the pulse period associated with that ground motion. These extensions improve the accuracy of PSHA for sites located near faults, as well as provide a rational basis for selecting appropriate near-fault ground motions to be used in the dynamic analyses of a structure. [DOI: 10.1193/1.2790487]

INTRODUCTION

In principle, when an earthquake fault ruptures and propagates towards a site at a speed close to the shear wave velocity, the generated waves will arrive at the site at approximately the same time, generating a "distinct" velocity pulse in the ground motion time history in the strike-normal direction (Singh 1985, Somerville et al. 1997). This intense velocity pulse usually occurs at the beginning of a record. This is referred to as the forward-directivity effect, which has been known for more than a decade to have the potential to cause severe damage in a structure (for example, Bertero et al. 1978, Singh 1985, Hall et al. 1995, Hall 1998, Hall and Aagaard 1998, Wald and Heaton 1998, Iwan 1999, Aagaard et al. 2000, Iwan et al. 2000, Aagaard et al. 2001, Alavi and Krawinkler 2001, MacRae et al. 2001). The question of how to estimate the ground motion hazard for a site that may experience such a forward-directivity effect is raised because not all

[a] Dept. of Civil & Environmental Eng., Stanford University, Stanford, CA 94305 (now at: AIR Worldwide Corporation, San Francisco, CA 94111)
[b] Professor Emeritus, Dept. of Civil & Environmental Eng., Stanford University, Stanford, CA 94305
[c] Assistant Professor, Dept. of Civil & Environmental Eng., Stanford University, Stanford, CA 94305

Earthquake Spectra, Volume 23, No. 4, pages 867–891, November 2007;

observed earthquake ground motions exhibit distinct velocity pulses when they are expected. Thus, probabilistic methods are used to quantify the effects of pulses in any given seismic environment. In the past, only a few available spectral acceleration attenuation relationships that account for the forward-directivity effect have been developed, e.g., Somerville et al. (1997), later modified by Abrahamson (2000). (It should be noted here that later, when we refer to the Somerville et al. 1997, we actually mean the attenuation model modified by Abrahamson [2000].) However, due to the limited samples of ground motions with distinct velocity pulses, such relationships were developed for a "broadband" directivity model. This broadband model simply decreases or increases the amplitudes of the spectral ordinates monotonically with respect to increasing period. Further, Somerville et al. (1997) used a data set consisting of both pulse-like records and others, smearing out the effect of the former.

Recent studies (e.g., Alavi and Krawinkler 2001, Mavroeidis and Papageorgiou 2003, Somerville 2003, Baker and Cornell 2005, Fu 2005, Tothong and Cornell 2006a, Tothong and Cornell 2007) have shown that a ground motion with a distinct velocity pulse tends to cause heightened elastic response only in a narrow period range of structures, namely those with a natural period close to the pulse period (T_p). As a result, it is important to develop a "narrowband" ground motion attenuation relationship, in which only spectral amplitudes around T_p are modified, in order to better characterize this special class of ground motions and its statistical properties. This paper will describe and demonstrate an approach for performing a probabilistic seismic hazard analysis (PSHA) that addresses explicitly records with such narrowband characteristics. Records without such pulses are treated separately. The paper will also highlight the information that needs to be developed and modified for this procedure.

This paper focuses on the pulse effect from forward directivity, and not on the permanent static ground motion displacement ("fling"), which is predicted to occur, for example, in the parallel component of a strike-slip mechanism. In reality, forward directivity and fling are coupled depending on the orientation of the fault and faulting style (Mavroeidis and Papageorgiou 2002, Bray and Rodriguez-Marek 2004).

GROUND MOTION RECORDS

The "pulse-like" ground motion recordings used in this study are a collection of the pulse motions identified by Mavroeidis and Papageorgiou (2003), Fu and Menun (2004), and Bazzurro and Luco (2004). The first two pairs of authors visually selected recordings deemed to contain a pulse in the velocity trace. Bazzurro and Luco (2004) selected records whose location relative to the fault rupture suggested that a velocity pulse was likely to occur, rather than directly identifying a velocity pulse in the record. As a result, we visually selected only the subset of their record set that appeared to contain a pulse. The first two author pairs fit a simple waveform with a modulating function to estimate the T_p, while Bazzurro and Luco (2004) used empirical mode decomposition (Loh et al. 2001) to estimate the T_p. The processed records in the fault-normal direction were obtained from the Next Generation Attenuation database as of March 2005 (NGA 2006). Ground motion records were selected from both firm soil and rock (based on Geomatrix site classes) for all faulting styles. This pooling of site and faulting sets is justifiable here

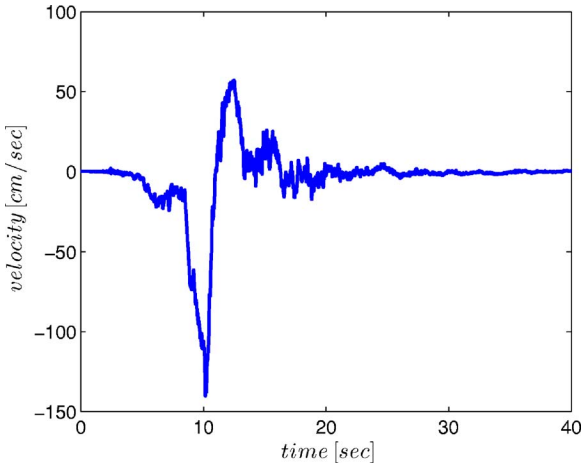

Figure 1. The velocity time history at Lucern station in the fault-normal direction during the 1992 Landers earthquake, demonstrating the forward-rupture-directivity effect.

because we expect that the pulse-like nature of these motions will dominate the spectral shape, and the spectral shape effects induced by other ground motion properties will be less influential.

It should be pointed out that the identification of pulse ground motions is not unique, varying from one researcher to another. In the interest of obtaining a larger sample size, we have included in the pulse-like set any recording that at least one of these authors has identified as such. A total of 70 pulse-like records is contained in the resulting sample. These recordings are listed in Tothong and Cornell (2006a; in Appendix A, Table A.2). These data are used here only to demonstrate the effects of such recordings and the application of the proposed PSHA procedure; the data set here does not affect the procedure per se. More systematic pulse-identification methods (Baker 2007) are under development for the purpose of developing numerical estimates of the pulse probabilities and narrowband attenuation relationships necessary for practical implementation of this method.

NARROWBAND PULSE-LIKE RECORDS

A near-fault (or near-source) pulse-like ground motion differs from a far-field motion by its "distinct" pulse in the velocity time history. Figure 1 shows an example ground motion recording that displays the forward-rupture-directivity effect in the fault-normal direction during the 1992 Landers earthquake. This velocity record shows a clear low-frequency (long-period) waveform of the pulse. It should be pointed out that estimating the pulse period (T_p) may in itself be a challenging problem due to noise present in accelerograms (Mavroeidis and Papageorgiou 2002). Rather than attempt to measure T_p by fitting a function to the velocity time history, we define T_p here as the period at the peak of the response spectral velocity (S_v) with 5% damping ratio. Past research has

shown that this T_p value generally provides a good estimate of the period of the primary pulse present in the ground motion velocity time history (e.g., Alavi and Krawinkler 2001, Fu and Menun 2004, Sinan et al. 2005). This estimation procedure ensures a common definition of T_p for the entire record set.

It has been shown that only oscillators within a narrow range of periods will be affected significantly differently by a pulse-like record with a given T_p; thus it is desirable to incorporate T_p in ground motion studies and structural analyses. It is particularly helpful to know the *relative* value between the period of the oscillator and the pulse period of the ground motion (Alavi and Krawinkler 2001, Mavroeidis et al. 2004, Fu 2005). Given this systematic behavior, it should prove valuable to incorporate T_p into PSHA. Including T_p as an extra variable will require some modifications in standard PSHA, as will be explained below.

The pulse-like ground motions were grouped into T_p bins ($0.25 \leq T_p < 0.65$, $0.65 \leq T_p < 1.5$, $1.5 \leq T_p < 2.5$, $2.5 \leq T_p < 3.5$, $3.5 \leq T_p < 4.5$) to illustrate the narrowband characteristics. The estimated mean values of T_p ($\bar{T}_p$) in each bin are about 0.4, 1.0, 1.9, 3.1, and 4.0 sec, and the number of records in each bin is 13, 20, 8, 10, and 9, respectively. These periods will be used below to indicate the specific bin used to generate data for plots and numerical examples. Figure 2 shows the estimated median (geometric mean) response spectra of the pulse-like motions from two different T_p bins. Also plotted in Figure 2 are median predictions of these spectra obtained from ordinary (Abrahamson and Silva 1997) and directivity-adjusted "broadband" (Somerville et al. 1997) ground motion prediction models. As can be seen from Figure 2, the median curves of the response spectra for the narrow T_p bins show peaks at periods around T_p and flatten back downward towards the median values of ordinary record as periods move away from T_p, exhibiting the so-called "narrowband" effect. This is a characteristic of forward-rupture-directivity ground motions, as confirmed by observations from recent large earthquakes (Somerville 2003). In contrast, the "broadband" model for these ground motions predicts larger response spectral values at a wide range of periods, rather than just a narrow range around T_p. When comparing the median curves in Figure 2 with the predicted median curves using Somerville et al.'s broadband model (1997), where all periods are monotonically modified, it is clear that there is an important difference. This observation emphasizes that pulse-like ground motions cannot be adequately described by the monotonic broadband scaling. To demonstrate further the narrowband directivity spectrum, we plotted the median acceleration and velocity spectra of the pulse-like ground motions that have been grouped into T_p bins. Figure 3 shows that only spectral periods near T_p are significantly amplified, while spectral periods further away from T_p are amplified less.

Figure 4 shows the estimated mean value of the normalized residuals (ε) of the pulse-like data (for four T_p bins) along with its $+/-$ one standard deviation bands calculated using the conventional attenuation relationship (i.e., Abrahamson and Silva 1997 model shown by a solid line and shaded area, respectively) and using the attenuation model accounting for the forward-directivity effect in the fault-normal component (dotted line; Somerville et al. 1997). Epsilon, ε, is defined as the number of standard devia-

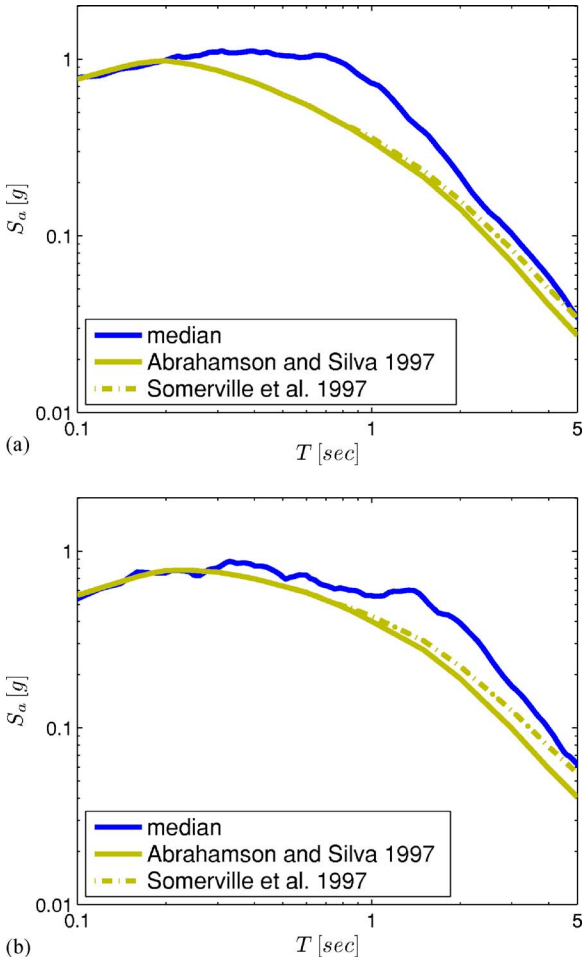

Figure 2. The empirical median response spectra of the pulse-like records along with the medians estimated from Abrahamson and Silva (1997) for ordinary records and from Somerville et al. (1997) for the forward-directivity effect in the fault-normal direction. T_p bins: (a) $\bar{T}_p = 1.0$ and (b) $\bar{T}_p = 1.9$. (Strictly, the predicted median curves are the median of the n estimated medians as each record $[i = 1, \ldots, n]$ has its own earthquake magnitude, source-to-site distance, and median.)

tions by which the ground motion deviates from the predicted median attenuation model. The horizontal axis is the normalized period (T/T_p). The large deviation of ε from zero (here about 1.5 at T/T_p near unity) indicates the lack of fit when using a current attenuation model to estimate ground motion amplitudes of the pulse-like motions. The systematic deviation of ε from zero is clear, suggesting that T_p is a good indicator for predicting the spectral ordinates of pulse-like motions. The mean estimate of the normalized residuals decays to zero as oscillator periods shift away from T_p. It should

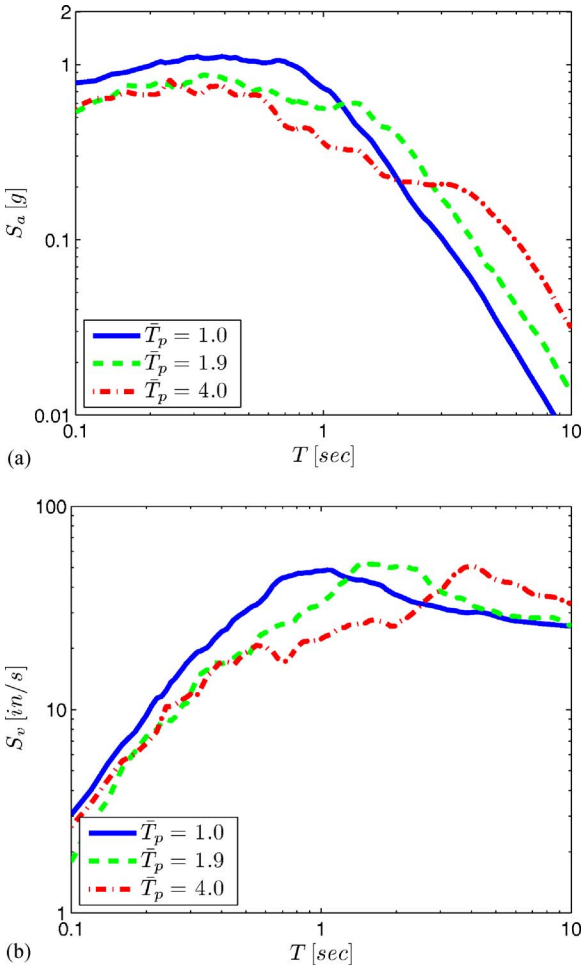

Figure 3. The median (a) acceleration spectra and (b) velocity spectra of the pulse-like ground motions from three T_p bins. For illustration, only three of the five bins are shown.

also be pointed out that ε calculated using Somerville et al. (1997) fails to capture the narrowband effect, as expected. Using Somerville's modification factor simply monotonically shifts the median ε toward zero, while the shape remains virtually unchanged. This figure confirms what is expected from the narrowband effect as pointed out by Somerville (2003). The T_p bin grouping demonstrates that the effect is similar for short-, intermediate-, and long-period pulses.

Figure 5 shows the histogram of the epsilon value, ε (i.e., a cross-section of Figure 4 at a specified T/T_p), using Abrahamson and Silva's model (1997), of both pulse-like and ordinary ground motions. The latter ground motion set was compiled by Tothong and Cornell (2006a; see Appendix A, Table A.3). From Figure 5, we notice that pulse-

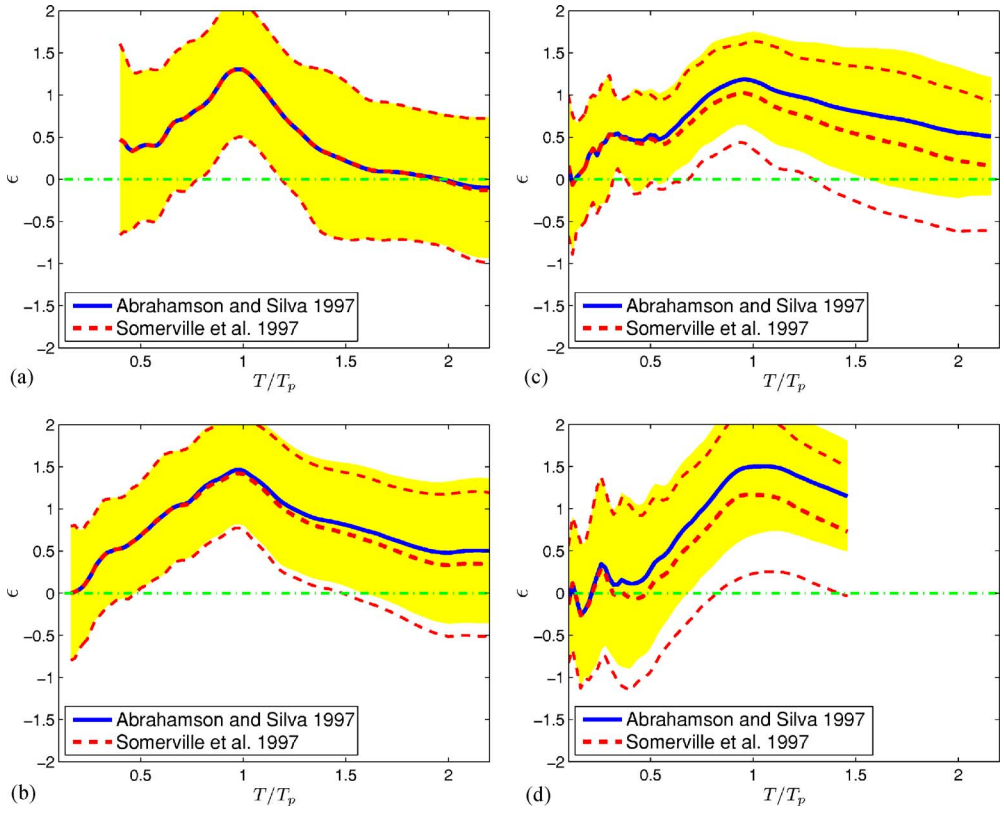

Figure 4. The ε values plotted versus the T/T_p grouped by T_p bins: (a) $\bar{T}_p$=0.4, (b) $\bar{T}_p$=1.0, (c) $\bar{T}_p$=1.9, and (d) $\bar{T}_p$=3.1. Solid and dotted lines are the median of the normalized residuals with respect to Abrahamson and Silva (1997) and Somerville et al. (1997) attenuation models, respectively. The shaded area and the thinner dotted lines are the +/- one standard deviation bands using Abrahamson and Silva (1997) and Somerville et al. (1997) attenuation models, respectively. The bin with $\bar{T}_p$=4.0 sec is similar.

like ground motions tend to have higher positive ε values than the ordinary records. This is because pulse-like ground motions are relatively strong for T/T_p=1.0 as compared to ordinary ground motions.

It should also be pointed out here that among the records typically identified as "near-source" based on their proximity to the fault, only a fraction will display a clear-cut, identifiable pulse-like behavior. Iervolino and Cornell (2007) find this fraction to depend upon magnitude and geometry, but seldom to exceed 30%. Therefore, recent statistical studies seeking to identify and quantify this narrowband effect using the entire body of all near-source records have proven largely ineffective, i.e., the residuals show no significant T/T_p dependence. The large fraction of non–pulse-like records in the near-source regime together with the broad scatter in the value of T_p tend to "smear out" and

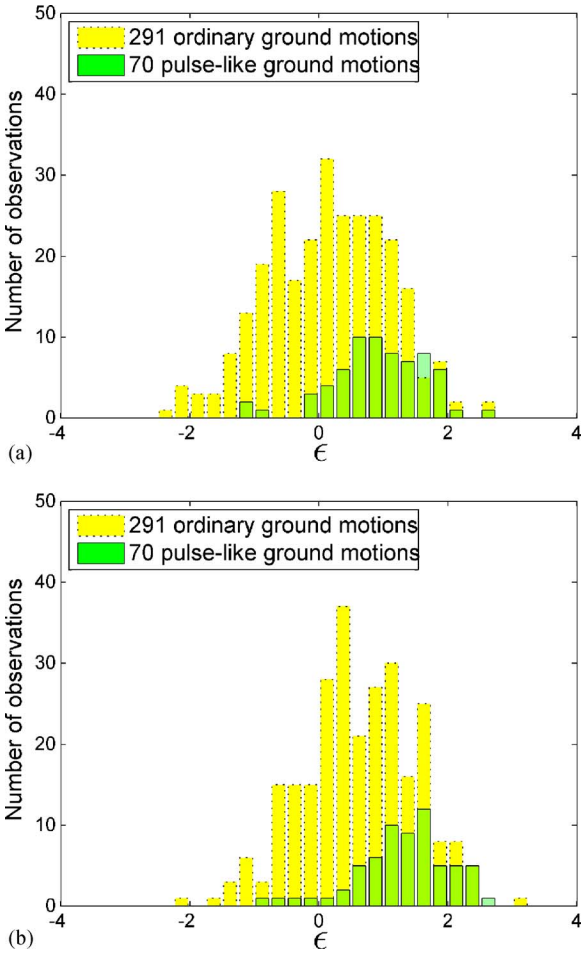

Figure 5. Histogram of epsilon at (a) $T/T_p=0.75$ and (b) $T/T_p=1.0$ for the pulse-like ground motion data set superimposed with that of ordinary earthquake records.

dampen the narrowband effect when looked at this way. In contrast, here we look only at the subset of records pre-identified as being pulse-like, when the effects are clear and quantifiable.

THE EFFECT OF PULSE-LIKE GROUND MOTIONS ON STRUCTURAL RESPONSE

To validate the importance of T_p and the differences between ordinary and near-field pulse-like motions, the inelastic displacement ratios (S_{di}/S_{de}) of nonlinear oscillators for both ground motion sets versus the absolute spectral period, T, are plotted. Interested readers are referred to, for example, Tothong and Cornell (2006a, 2006b) for further explanation of S_{di}/S_{de} and its significance. The bilinear oscillator (with 5% hardening stiff-

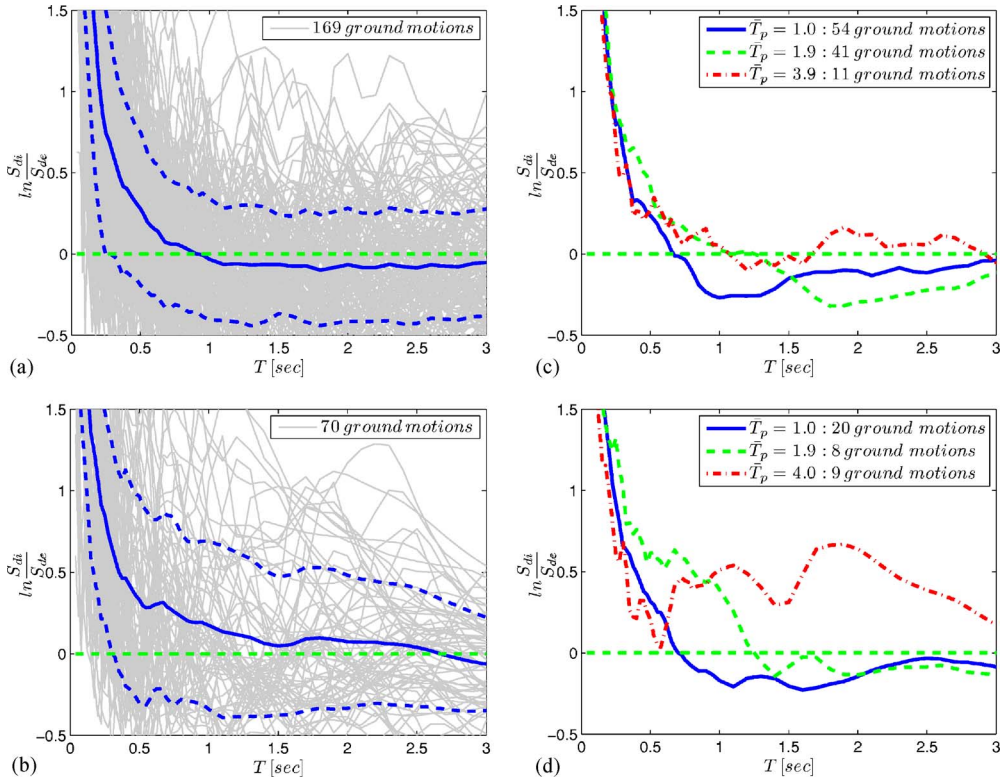

Figure 6. The $\ln(S_{di}/S_{de})$ with strength reduction factor equals 4 for (a) 169 ordinary ground motions, (b) 70 pulse-like ground motions, (c) mean values of ordinary ground motions grouped by T_p, and (d) mean values of pulse-like ground motions grouped by T_p.

ness and 5% damping ratio) responses, given by the inelastic spectral displacement (S_{di}) normalized by its elastic spectral value (S_{de}) at the same initial elastic period, are plotted in Figure 6 for a strength reduction factor equal to four. For inelastic responses, $T/T_p = 0.5$ (i.e., a T_p that is twice as long as the elastic period of an oscillator) seems to be the most damaging case because the effectively elongated period drifts towards the peak of the elastic spectrum, which is near the pulse period, T_p (e.g., Alavi and Krawinkler 2001, Mavroeidis et al. 2004, Fu 2005, Tothong and Cornell 2006a, Tothong and Cornell 2007). For the ordinary ground motion set, only ground motions with high-pass filter frequency less than or equal to 0.10 Hz are used to plot S_{di}/S_{de} shown in Figure 6. This removal of records with weak signals at long periods reduces the number of records from 291 to 169 accelerograms.

Figure 6a and Figure 6b show S_{di}/S_{de} for the ordinary and pulse-like ground motions, respectively. It is clear that the estimated mean (solid lines) and +/− one standard deviation (dotted lines) of $\ln(S_{di}/S_{de})$ of the pulse-like data set are higher for periods that range from 0.5 to 3.0 sec, resulting in a broadband-like modification factor. (ln(·) De-

notes the natural logarithm of (·) throughout.) But Figure 6d (for three T_p bins) demonstrates that S_{di}/S_{de} of a near-fault ground motion at a given period can be more precisely predicted if T_p is known. For example, for an oscillator with T=2 sec, the estimated mean value of $\ln(S_{di}/S_{de})$ is approximately 0.1 for the broadband model (Figure 6b), while it is approximately −0.2 for T_p=1 or 2 sec and approximately 0.7 for T_p=4 sec (Figure 6d). As shown in Figure 6c, knowing T_p for ordinary ground motions does not significantly help improve the characterization of the inelastic responses of nonlinear oscillators, so it is not useful to identify T_p for non–pulse-like motions (recall that T_p, the period at the peak of S_v, is defined for even non–pulse-like records).

Another example to illustrate the benefit of considering T_p in characterizing pulse-like, but not ordinary, ground motions is shown in Figure 7. The solid lines represent the correlation between $\ln S_a$ at two periods when considering all records. The dotted lines represent the correlation between $\ln S_a$ at two periods (T_1=2 sec and T_2 versus T_2) for ground motions with T_p values between 3.5 and 4.5 sec. For ordinary ground motions (Figure 7a), we observe that the correlation function does not change whether using all ground motions or only ground motions with T_p close to 4 sec. As seen in Figure 7b, however, the correlation of $\ln S_a$ for all pulse-like ground motions may differ dramatically from the correlation when using ground motions grouped by T_p bin. The correlation function between $\ln S_a$ at two periods can be used to develop the vector-valued PSHA (Bazzurro and Cornell 2002) for the near-fault environment in order to couple with the vector intensity measure (e.g., Shome 1999) to improve the probabilistic response prediction of structures.

PSHA METHOD

PSHA CONSIDERING NEAR-SOURCE EFFECTS

Given the above results that indicate differences between near-source and ordinary ground motions, it would be desirable to modify the PSHA to incorporate these effects in a hazard analysis. In order to clarify the effort needed and outline the differences for the pulse-like PSHA with the conventional PSHA (Cornell 1968, Reiter 1990, Frankel et al. 1996), we start with the following equation, which underlies the current standard approach for computing the mean annual frequency (MAF, $\lambda_{S_a}(x)$) of exceeding a ground motion parameter level, e.g., elastic-pseudo spectral acceleration (S_a) exceeding an intensity level x:

$$\lambda_{S_a}(x) = \sum_{i=1}^{\#\ faults} \nu_i \int_{m_w, r_{rup}} (G_{S_a|M_w^i, R_{rup}^i}(x|m_w, r_{rup})) \cdot f_{M_w^i, R_{rup}^i}(m_w, r_{rup}) \cdot dm_w \cdot dr_{rup} \quad (1)$$

where ν_i is the mean rate of occurrence of earthquakes on fault i above a minimum threshold magnitude. Uppercase denotes random variables, and lowercase indicates realizations of those random variables throughout this paper. M_w is the moment magnitude and R_{rup} is the closest distance from the site to the rupture plane. $f_{M_w^i, R_{rup}^i}(m_w, r_{rup})$ is the joint probability density function (PDF) of M_w and R_{rup} on fault i. G_{S_a} is the Gaussian

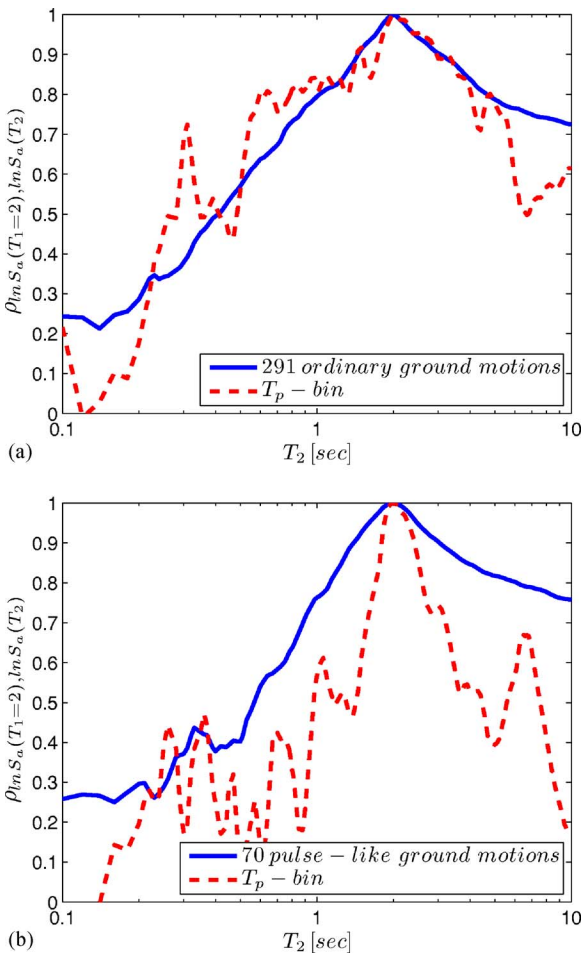

Figure 7. The correlation of spectral acceleration between two spectral periods, T_1=2 sec and T_2 versus T_2, when using records with T_p values between 3.5 to 4.5 seconds: (a) ordinary ground motions and (b) pulse-like ground motions.

complementary cumulative distribution function (CCDF) of the lognormally distributed random variable S_a, which is defined as

$$G_{S_a|M_w^i,R_{rup}^i}(x|m_w,r_{rup}) = 1 - \Phi\left(\frac{\ln x - \mu_{\ln S_a|m_w,r_{rup}}}{\sigma_{\ln S_a|m_w,r_{rup}}}\right) \tag{2}$$

where $\Phi(\cdot)$ is the standard Gaussian CDF, and $\mu_{\ln S_a|m_w,r_{rup}}$ and $\sigma_{\ln S_a|m_w,r_{rup}}$ are the conditional mean and standard deviation of the natural logarithm of S_a, as obtained from a ground motion attenuation model (e.g., Abrahamson and Silva 1997).

Building upon the above standard implementation of PSHA, it is now necessary to

make several modifications to incorporate the effect of near-fault directivity. As in Somerville et al. (1997), we introduce a directivity parameter (X (or S)$\cdot\cos\theta$), where $X = S/L$; S is the projected distance (along the rupture plane) from the epicenter toward the site; L is the fault rupture length; and θ is the azimuth angle between the fault rupture plane and the direction between the epicenter location and the site (Somerville et al. 1997). A similar definition is also available for the non–strike-slip case. In current near-source PSHA software, the location of the hypocenter is treated as random, inducing a distribution on $S\cdot\cos\theta$ and requiring in effect an additional level of integration. Below, for notational simplicity, we denote $S\cdot\cos\theta$ as Z, implying too that the formulation is independent of exactly how this variable is defined. In addition, we now propose to condition the prediction of S_a on T_p, and then to integrate over the distribution of possible T_p realizations. In addition, we chose to narrow our attention to pulse-like records because, as we have seen above, they impact linear and nonlinear structural response in predictable ways. This additional restriction implies the need to develop an empirical relationship for the likelihood of observing a pulse-like ground motion given record properties, $P[pulse|\ M_w, distance, directivity\ parameters, \text{etc.}]$. This piece of information is currently under development by Iervolino and Cornell (2007).

Once all of the pieces of information have been established, we can incorporate the near-source (NS) pulse-like effect into the PSHA using the following equation:

$$\lambda_{S_a}(x) = \lambda_{S_a,non-NS}(x) + \lambda_{S_a,NS}(x) \tag{3}$$

where $\lambda_{S_a,non-NS}$ is simply that shown in Equation 1 for non–near-source hazard, e.g., for distances greater than, say, 20 km. The MAF of S_a for the near-source case ($\lambda_{S_a,NS}$) is given as follows, where $\lambda_{S_a,NS}$ is separated into two parts: the near-source hazard from the narrowband pulse-like ground motion events ($\lambda_{S_a,NS\&pulse}$), and the near-source hazard due to non–pulse-like records ($\lambda_{S_a,NS\&no\ pulse}$).

For a given fault within $R_{rup} < 20$ km,

$$\lambda_{S_a,NS}(x) = \lambda_{S_a,NS\&pulse}(x) + \lambda_{S_a,NS\&no\ pulse}(x) \tag{4}$$

in which (assuming for simplicity only a single fault):

$$\lambda_{S_a,NS\&pulse}(x) = \int_{m_w,r_{rup}} \int_z P(pulse|m_w,r_{rup},z) \cdot \int_{t_p} G_{S_a|pulse,M_w,R_{rup},Z,T_p}(x|m_w,r_{rup},z,t_p) \cdot f_{T_p|Z,M_w,R_{rup}} \cdot f_{Z|M_w,R_{rup}} \cdot dt_p \cdot dz \cdot \left|d\lambda_{M_w,R_{rup}}(m_w,r_{rup})\right| \tag{5}$$

$$\lambda_{S_a,NS\&no\ pulse}(x) = \int_{m_w,r_{rup}} \int_z G_{S_a|M_w,R_{rup},No\ Pulse}(x|m_w,r_{rup}) \cdot (1 - P(pulse|m_w,r_{rup},z)) \cdot f_{Z|M_w,R_{rup}} \cdot dz \cdot \left|d\lambda_{M_w,R_{rup}}(r_{rup},m_w)\right| \tag{6}$$

Note that $\int_{m_w,r_{rup}}[\bullet]\cdot\left|d\lambda_{M_w,R_{rup}}(m_w,r_{rup})\right| = \nu\cdot\int_{m_w}\int_{r_{rup}}[\bullet]\cdot f_{M_w,R_{rup}}\cdot dm_w\cdot dr_{rup}$, where

$|d\lambda_{M_w,R_{rup}}(r_{rup},m_w)|$ is the absolute value of the joint mean rate of occurrence of events with (loosely speaking) $M_w=m_w$ and $R_{rup}=r_{rup}$ on this nearby fault and ν is the mean rate of events on this fault. dt_p and dz are the integration intervals of the realization values of variable T_p and $Z(=S\cdot\cos\theta)$, respectively. $G_{S_a|pulse,M_w,R_{rup},Z,T_p}$ is the Gaussian CCDF of S_a conditioned on M_w, R_{rup}, Z, and T_p (or T/T_p), where T is the period of the oscillator. This narrowband S_a attenuation model is under development by NGA (e.g., Youngs and Chiou, personal communication with the authors, 2006). f_{M_w,R_{rup},Z,T_p} is the joint PDF of M_w, R_{rup}, Z, and T_p. Similarly, $f_{M_w,R_{rup},Z}$ is the joint PDF of M_w, R_{rup}, and Z. Using the definition of conditional probability, the joint distribution f_{M_w,R_{rup},Z,T_p} in Equation 5 can be broken down as $f_{T_p|M_w,R_{rup},Z}\cdot f_{Z|M_w,R_{rup}}\cdot f_{M_w,R_{rup}}$. However, T_p has been found to depend only on M_w (as cited above); therefore the function $f_{T_p|M_w,R_{rup},Z}$ is reduced to simply $f_{T_p|M_w}$.

To compute $\lambda_{S_a,NS\&no\ pulse}(x)$ in Equation 4, it may be possible to use the same attenuation relationships (for the ordinary ground motions) for $R_{rup}<20$ km and $R_{rup}\geq 20$ km, but this must be confirmed as these $R_{rup}<20$ km non–pulse-like motions are likely to have smaller median and standard deviation values than the current S_a attenuation models because they exclude the ground motions within 20 km with the severe pulse-like motions. Youngs and Chiou (personal communication with the authors, 2006) are also investigating this issue.

For a fault with $R_{rup}\geq 20$ km, the conventional PSHA (shown in Equation 1) can be used to compute $\lambda_{S_a,non-NS}(x)$ because large-amplitude pulse-like ground motions, while not impossible, are not likely there. In effect, we carry out the above three PSHAs—namely $\lambda_{S_a,non-NS}(x)$, $\lambda_{S_a,NS\&pulse}(x)$, and $\lambda_{S_a,NS\&no\ pulse}(x)$—and sum them to obtain the total site-specific ground motion hazard.

PSHA DISAGGREGATION

In addition to the hazard curves considered above, another common calculation in PSHA is disaggregation (McGuire 1995, Bazzurro and Cornell 1999). Typically, this calculation is used to compute the distribution of magnitudes, distances, and epsilon values contributing to occurrence or exceedance of some ground motion intensity level. In this section, disaggregation equations are developed to also provide the probability that a ground motion intensity level is caused by a pulse-like ground motion, and to provide the distribution of pulse periods associated with those ground motions. This disaggregation is important to structural engineers because it provides a rational basis for selecting representative ground motions (near-fault and non–near-source) to be used in dynamic analyses of a structure.

To compute the probability that a ground motion with S_a *equaling* x is caused by a pulse-like ground motion, the following application of Bayes' theorem can be used:

$$P[pulse|S_a=x]=\frac{\Delta\lambda_{S_a,NS\&pulse}(x)}{\Delta\lambda_{S_a}(x)} \tag{7}$$

where $\Delta\lambda_{S_a}(x)=\lambda_{S_a}(x)-\lambda_{S_a}(x+\Delta x)$ and Δx is a small increment of S_a.

Once the probability of experiencing pulse-like motions is known ($P[pulse|S_a]$), it would be helpful to know the distribution of associated pulse periods because (as mentioned above) the pulse period will affect the resulting structural responses. The following equation can be used to obtain the PDF of T_p conditioned on S_a equaling x and on experiencing a pulse-like motion:

$$\begin{aligned} f_{T_p|S_a=x,pulse} &\propto \frac{P[T_p=t_p, S_a=x, pulse]}{P[S_a=x, pulse]} \\ &= \left\{ \int_{m_w,r_{rup}} \int_z \Delta G_{S_a|M_w,R_{rup},Z,T_p}(x|m_w,r_{rup},z,t_p) \right. \\ &\quad \cdot P[pulse|m_w,r_{rup},z] \cdot f_{T_p|M_w,R_{rup},Z} \cdot f_{Z|M_w,R_{rup}} \\ &\quad \left. \cdot dz \cdot |d\lambda_{M_w,Rrup}(m_w,r_{rup})| \right\} \Big/ \Delta\lambda_{S_a,NS\&pulse}(x) \end{aligned} \quad (8)$$

where $\Delta G_{S_a|\bullet}(x|\bullet) = G_{S_a|\bullet}(x|\bullet) - G_{S_a|\bullet}(x+\Delta x|\bullet)$.

EXAMPLE

We demonstrate the proposed PSHA framework and the potential effects of near-source effects by considering two hypothetical seismic cases: a firm soil site located at R_{rup}=3 km from a strike-slip fault that produces only characteristic M_w=6.0 events, and another separate example in which the site is 14 km from a fault that produces only M_w=7.5 events. For simplicity the mean annual rate of the characteristic earthquakes for both cases is assumed to be unity. In both cases, the site location projected onto the fault rupture plane is assumed to be in the middle of the fault. To incorporate directivity parameters, we assume that the epicenter location follows a uniform distribution along the fault. The fault lengths are eight and 100 kilometers. For non–pulse-like records, we used the Abrahamson and Silva (1997) attenuation relationship. For pulse-like ground motions, a narrowband modification function was estimated from data shown in Figure 4. The Harversed sine function was used to fit the normalized residuals by increasing the median value (for $0.5 \le T/T_p \le 1.5$); the dispersion was assumed to remain unchanged. The empirical model used to estimate $f_{T_p|M_w}$ follows a lognormal distribution, which is similar to the one shown in Somerville (2003). The estimated median values of T_p($\hat{T}_p$) for the M_w=6.0 and 7.5 events are 0.7 and 4.7 sec, respectively. The standard deviation of ln T_p given M_w ($\sigma_{\ln T_p|M_w}$) is 0.7 in both cases. To approximate a continuous distribution, the realizations of T_p are varied from 0.1 to 15 sec using small, 0.1-second, intervals. Finally, the probability of a pulse occurring at the site given an event that was used here was based on early exploratory analyses by Iervolino and Cornell (2007), who found empirically that $P[pulse|M_w,R_{rup},S,\theta] = 1/(1+\exp(-(b_0+b_1\cdot R_{rup}+b_2\cdot S+b_3\cdot\theta+b_4\cdot(R_{rup}\times\theta)+b_5\cdot(S\times\theta))))$, with b_0=−4.589, b_1=−3.914, b_2=4.046, b_3=−4.923, b_4=−2.883, b_5=4.190.

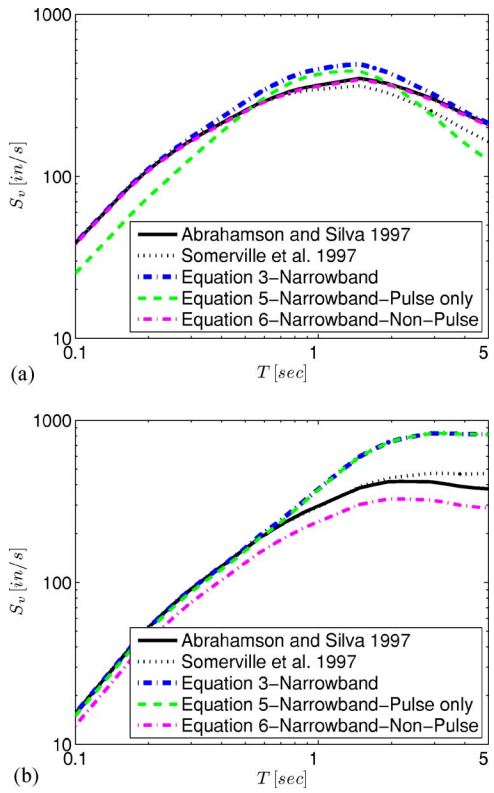

Figure 8. UHS at MAF of exceeding S_v at 1% in 100 years for (a) M_w=6.0 and (b) M_w=7.5.

UNIFORM HAZARD SPECTRA

The target MAF of exceeding S_a is chosen to be 1% in 100 years. The uniform hazard spectra (UHS) of the two cases are shown in Figure 8. The thick solid line represents the UHS using Abrahamson and Silva (1997). The thick dotted line represents the total hazard using the proposed narrowband Equation 3. The dashed and dashed-dotted lines represent MAF using Equations 5 and 6, respectively, i.e., they are the two contributions to the near-source hazard. The broadband directivity attenuation model (Somerville et al. 1997) is also shown (thin dotted lines). When compared to the models of Abrahamson and Silva (1997) and Somerville et al. (1997), the proposed PSHA framework demonstrates a more intuitive picture of how narrowband pulse-like motions will affect the computed ground motion hazard. Note that in Figure 8a the narrowband UHS is equal to the Abrahamson and Silva–based UHS at shorter and longer periods, amplifying it only in a region of T centered on 0.5 to 2 sec. This narrowband effect exists but is not so obvious in Figure 8b because the UHS computations are restricted by current attenuation law limitations to $T<5$ sec. Periods significantly longer than the expected T_p of 4.7 sec,

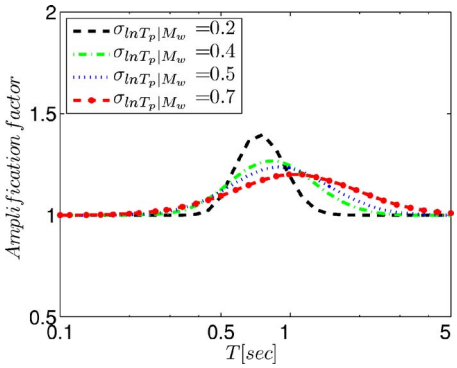

Figure 9. Amplification factor for M_w=6.0 event.

therefore, cannot be shown. The UHS shows its largest amplification relative to Abrahamson and Silva (1997) at the T close to $\hat{T}_p$, i.e., 0.7 and 4.7 seconds for M_w=6.0 and 7.5, respectively.

EFFECT OF $T_P|M_W$ DISTRIBUTION

As the introduction of T_p is what distinguishes this narrowband model from previous broadband models, in this section we explore the role of the conditional distribution of T_p given M_w on the near-source UHS. In the previous section we saw the effect of changes in the median of T_p due to changes in the causative magnitude. In Figure 9, we show (for the M_w=6.0 case) the ratio (amplification factor) of the UHS for the narrowband approach versus that from the simple Abrahamson and Silva (1997) prediction. Note that as $\sigma_{\ln T_p|M_w}$ increases, this amplification broadens, has a lower peak, and has a peak at a longer period.

To illustrate more graphically the effect of $\sigma_{\ln T_p|M_w}$ on the UHS, we assume next two different $\sigma_{\ln T_p|M_w}$ values: 0.7 and 0.2. The median value of T_p is 4.7 (for the M_w=7.5 case). In order to help visualize the effect of the narrowband modification, we use here a coarse, discrete, three-mass approximation of the T_p distribution (T_p=2.3, 4.7, and 7.0 sec). These three T_p values are assigned the appropriate probability mass function (PMF) obtained from $f_{T_p|M_w}$. For $\sigma_{\ln T_p|M_w}$=0.7, the PMF for each T_p realization is 0.34, 0.28, and 0.38, respectively. The PMF is 0.08, 0.79, and 0.13, respectively, for $\sigma_{\ln T_p|M_w}$=0.2.

Noticeably, the smallest T_p realization will be given a very different weight according to how large $\sigma_{\ln T_p|M_w}$ is. This will affect the narrowband amplification at those periods. The unifrom hazard spectra using these two three-mass T_p approximations are shown below in Figure 10 for the case of one fault producing only M_w=7.5 events. The S_a or S_v amplification relative to Abrahamson and Silva (1997) is shown in Figure 11 for three different cases: the S_v amplification for 1) Figure 8b, 2) Figure 10a, and 3) Figure 10b. The amplification is calculated as the ratio of S_v from the UHS based on the nar-

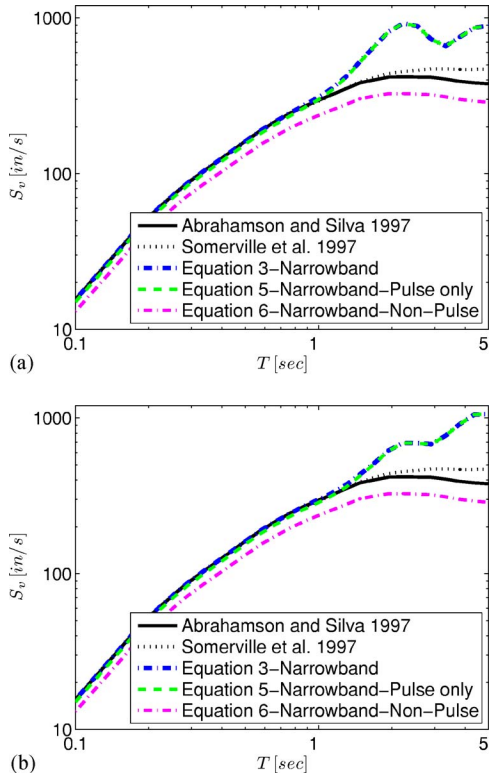

Figure 10. S_v UHS using three T_p realizations for M_w=7.5: (a) with $\sigma_{\ln T_p|M_w}$=0.7, (b) with $\sigma_{\ln T_p|M_w}$=0.2.

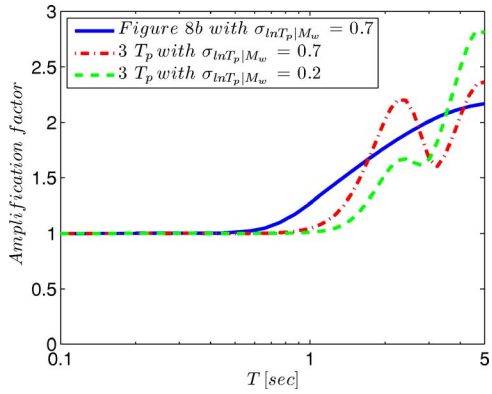

Figure 11. Amplification factor for M_w=7.5 event.

rowband modification (Equation 3) to S_v from the UHS that uses only Abrahamson and Silva (1997) for all periods and events. Note that the three-mass representation with $\sigma_{\ln T_p|M_w}=0.7$ produces a "lumpy" approximation to the continuous result. As shown in Figure 9 and Figure 11, the peak amplification value is dictated by the effect of $\sigma_{\ln T_p|M_w}$. The larger the $\sigma_{\ln T_p|M_w}$, the more the shift in the peak amplification to the right (longer period). The smaller the $\sigma_{\ln T_p|M_w}$, the narrower the amplification and the higher the peak. Even with $\sigma_{\ln T_p|M_w}=0.2$, however, there remains a significant amplification of the UHS at $T\approx 2$ sec. Indeed it must be remembered that the UHS is a weighted combination of possible future events. No matter what $\sigma_{\ln T_p|M_w}$ may be, individual spectra observed during these future events will have comparatively narrow response spectra with, potentially, a peak near, say, 2 sec. The lowering and widening of the UHS with increased $\sigma_{\ln T_p|M_w}$ is a product of the UHS "averaging" process.

DISAGGREGATION OF PSHA RESULTS

Here we use Equations 7 and 8 to compute the probability of a pulse and the distribution of T_p values, *conditional* upon $S_a=x$. In Figure 12a, conditional distributions of T_p results (Equation 8) are shown for $S_a=0.4$ g at $T=2$ sec using the $M_w=7.5$ source example case. Similar results are shown in Figure 12b for an S_a level of 3.0 g. These values of x correspond to annual probabilities of exceedance of 32% and 0.24% for this example case. The probabilities of these values "due to" a pulse are 0.75 and 0.97, respectively (Equation 7). The former S_a level (0.4 g) represents an epsilon of about 0.6 relative to the median spectral acceleration predicted by Abrahamson and Silva (1997), which in effect assumes no pulse, while the latter value represents an epsilon of 3.5 if there were no pulse. Figure 13 presents similar results for the $M_w=6.0$ illustration. The levels of 2-sec S_a being conditioned upon here are 0.2 and 1.5 g. These levels correspond to annual probabilities of 3.6% and 0.086%, respectively, the probabilities that were associated with a pulse occurrence are 0.08 and 0.23, respectively, and the epsilons are 0.3 and 2.8 relative to Abrahamson and Silva (1997). Based on these no-pulse epsilons, the lower values are not exceedingly rare (given an event) whereas the higher two values are—unless a pulse occurs and its period is such that it induces larger median ground motion amplitudes at the T of interest. Therefore, the occurrence of a larger ground motion amplitude "suggests" that a pulse occurred and increased the median prediction, i.e., that the pulse period was not far from the period of interest.

These effects dictate the Figure 12 and Figure 13 shapes of the disaggregated T_p distributions, i.e., the conditional distributions given $S_a=x$. The left-hand sides (lower S_a values) are similar in shape to the marginal distributions of T_p (i.e., here, the lognormal distributions given $M_w=7.5$ or 6.0). The right-hand sides (higher S_a values), on the other hand, show sharp conditional probability mass increases near the period of interest.

It is anticipated that these disaggregation results will be of particular use in guiding the selection of sample ground motion recordings for use in nonlinear dynamic foundation and structural analysis.

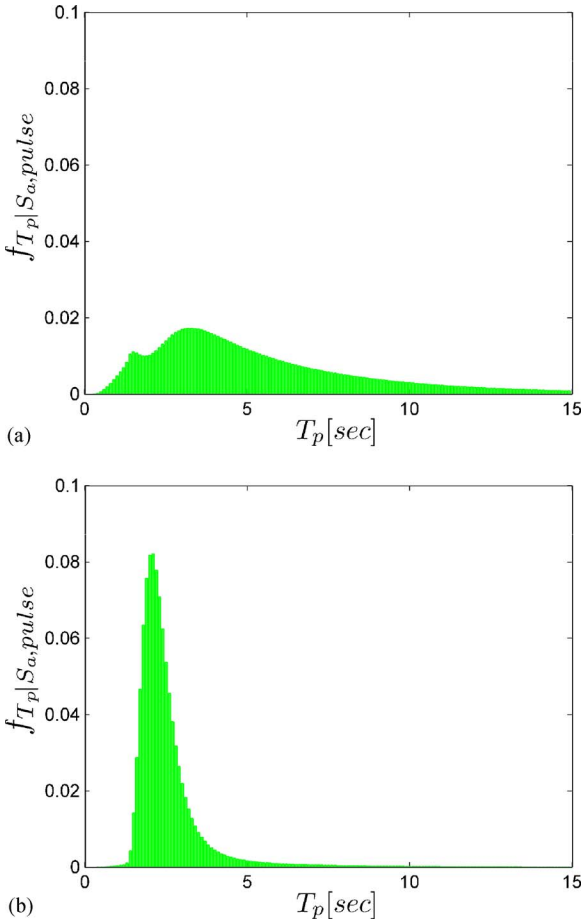

Figure 12. Conditional probability density functions for T_p, given $S_a=x$ and a pulse-like ground motion for M_w 7.5: (a) $S_a=0.4$ g and (b) $S_a=3.0$ g for $T=2$ sec.

DISCUSSION

This paper has presented an explicit pulse–based PSHA method in terms to S_a, elastic spectral acceleration, as the scalar ground motion intensity measure. It appears in the development of the equations as well as in the illustrations. This intensity measure was chosen because it is the conventional and most familiar one. The PSHA then provides conventional uniform hazard spectra as well as insights from the disaggregation by pulse and pulse period that supplement the conventional M_w, R_{rup}, and epsilon disaggregation results. Together these results can be used much as they are now for near-source sites to aid in the selection and scaling of recordings for use in foundation and structural dynamic analyses, e.g., to estimate the probability distribution of response given an S_a value with a specified mean annual frequency. This may mean scaling to that S_a level a sample of records chosen to reflect the causative magnitude, distance, and epsilon range,

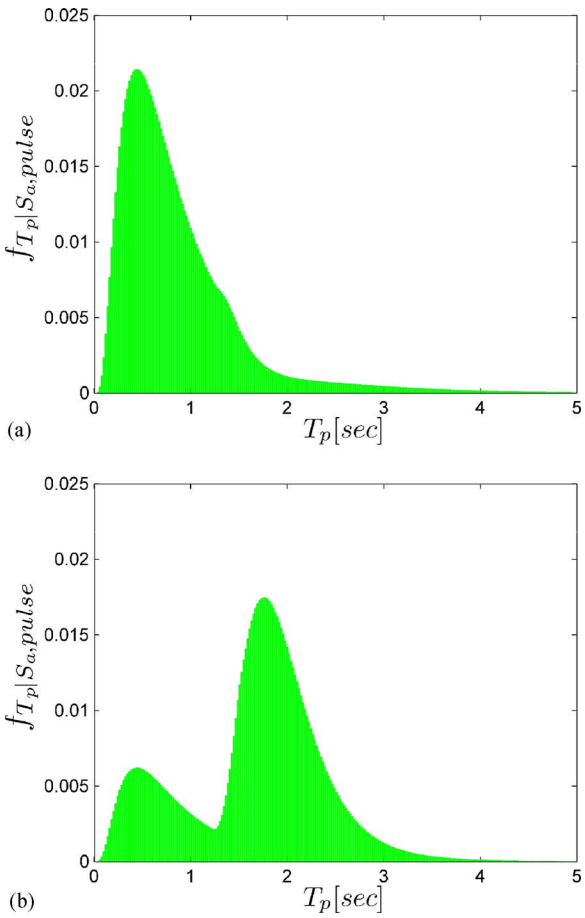

Figure 13. Conditional probability density functions for T_p, given $S_a=x$ and a pulse-like ground motion for M_w 6.0: (a) $S_a=0.2$ g and (b) $S_a=1.5$ g for $T=2$ sec.

plus, now, to reflect the correct fraction of pulse-like records together with their appropriate range of T_p values. In this way the effects of pulse-like records on, for example, nonlinear response (described earlier) will be captured and their contribution to the seismic threat ascertained. Analogous to the procedures that have been developed to deal with the (local) peak-valley or "epsilon" effect (Baker and Cornell 2005, 2006), careful record selection, and/or weighting, and/or local regression techniques may all help make the assessment of structural response distributions easier in the near-source case as well, although the dimensionality has been increased to include T_p. These procedures all require disaggregation results. For example, at 3.0 g intensity with $M_w=7.5$, if the total ground motion needed is 30 records, engineers will then select 29 (i.e., 0.97×30) pulse-

like ground motions with T_p values that approximately match the distribution in Figure 12b and one non-pulse ground motion matching the S_a disaggregation on ε (probably the mean value in this case).

While written for S_a, the PSHA equations (e.g., Equation 3) also hold if S_a is replaced by virtually any other candidate scalar intensity measure (IM). In particular, they hold if elastic S_a is replaced by S_{di}, which has been shown (Luco 2002, Tothong and Cornell 2006a, Luco and Cornell 2007, Tothong and Cornell 2007, Tothong and Luco 2007) to be a very effective IM. With S_{di} as the IM in the explicit-pulse PSHA, again an attenuation law for pulse-like ground motions would need to be created. The robustness that S_{di} has shown with respect to pulse-like ground motions in the past (e.g., Tothong and Cornell 2006a, Tothong and Cornell 2007, Tothong and Luco 2007) suggests that the (S_{di}–based) epsilon versus T/T_p plots parallel to Figure 4 would be significantly different, with the mean lying closer to zero for all T/T_p. This robustness also suggests that the shape of $f_{T_p|pulse,S_{di}}$ would be less sensitive to the ground motion amplitude level and to T_p. All this muting of the pulse effects implies that record selection and scaling should be simpler if S_{di} is used as the IM. Some of these same conclusions may also prove true for IMs such as S_{a-AVG}, the spectral acceleration averaged over a relevant frequency band. Finally, extension of the explicit-pulse PSHA to a vector IM such as $<S_a, \varepsilon>$ or $<S_a, \varepsilon, T_p>$ is also straightforward in principle.

CONCLUSIONS

A framework is proposed to incorporate accurately the effect of near-source pulse-like ground motions into probabilistic seismic hazard analysis. The framework explicitly incorporates the likelihood of experiencing pulse motions and the corresponding distribution of pulse periods, T_p, into the analysis. The PSHA is separated into two parts: non–near-source contribution and the near-source contribution. The former is simply a conventional PSHA. The latter, or near-source, contribution is separated further into that due to the event of experiencing a pulse-like motion and that when a pulse is not in evidence. For the pulse case, a new narrowband modification for the ground motion attenuation model needs to be developed. For the non-pulse but near-source case, the available attenuation models may require at most minor parameter value changes.

The direct output of the analysis includes intensity measure hazard curves and uniform hazard spectra. To improve seismic hazard assessments, disaggregation results provide the conditional distributions of the causative event variables (i.e., ε, M_w, *distance*, $P[pulse]$, T_p, etc.) that are associated with a ground motion at a given intensity level. In the same way that M_w, *distance*, and ε disaggregation are provided in standard PSHA, the near-source PSHA framework can provide disaggregation information for $P[pulse]$ and T_p distribution for a specified ground motion intensity level. This disaggregation information is important in selecting historical earthquake ground motions for structural analyses because it improves the understanding of earthquakes and their effects on structures. The method is illustrated with elastic spectral acceleration as the intensity measure using a simplified, preliminary model for the narrowband, pulse-like ground motion model. The disaggregation results of $P[pulse]$ and the conditional T_p distribution are shown to vary with the intensity level.

Once a PSHA analysis using the proposed procedure is complete and implemented, it will not require additional effort from the engineers. It is simply a modification to, e.g., the USGS hazard maps, together with supplementary information provided by disaggregation regarding the contribution of pulse-like ground motions to the seismic hazard. This extension will improve the usefulness and accuracy of PSHA results at sites that might be subjected to near-source ground motions with pulse-like, forward-directivity effects.

ACKNOWLEDGMENTS

The financial support for this research is provided by the National Science Foundation through the U.S.-Japan Cooperative Research in Urban Earthquake Disaster Mitigation Project (NSF 98-36) under grant number CMS-0200436, and NSF under Award Number EEC-9701568 through Pacific Earthquake Engineering Research (PEER) Center. This support is gratefully acknowledged. The first author would like to thank Jack Baker for reviewing, editing grammatical errors, and providing comments on the early draft of this paper. The mathematical derivations and analyses were performed by the first two authors.

REFERENCES

Aagaard, B. T., Hall, J. F., and Heaton, T. H., 2000. Sensitivity study of near-source ground motion, *Proceedings of the 12th World Conference on Earthquake Engineering, New Zealand Society for Earthquake Engineering*, Upper Hutt, New Zealand.

——, 2001. Characterization of near-source ground motions with earthquake simulations, *Earthquake Spectra* **17**, 177–207.

Abrahamson, N. A., 2000. Effects of rupture directivity on probabilistic seismic hazard analysis, *Proceedings of the Sixth International Conference on Seismic Zonation: Managing Earthquake Risk in the 21st Century*, Palm Springs, CA, 12–15 November 2000.

Abrahamson, N. A., and Silva, W. J., 1997. Empirical response spectral attenuation relations for shallow crustal earthquakes, *Seismol. Res. Lett.* **68**, 94–127.

Alavi, B., and Krawinkler, H., 2001. *Effects of Near-Field Ground Motion on Frame Structures*, John A. Blume Earthquake Engineering Center, Report No. *138*, Department of Civil and Environmental Engineering, Stanford University, CA, available at: http://blume.stanford.edu/Blume/TRList.htm [accessed 31 May 2006].

Baker, J. W., 2007. Quantitative classification of near-fault ground motions using wavelet analysis, *Bull. Seismol. Soc. Am.*, in review.

Baker, J. W., and Cornell, C. A., 2005. *Vector-Valued Ground Motion Intensity Measures for Probabilistic Seismic Demand Analysis*, John A. Blume Earthquake Engineering Center, Report No. *150*, Stanford University, CA, available at: http://blume.stanford.edu/Blume/TRList.htm [accessed 31 May 2006].

——, 2006. Spectral shape, epsilon and record selection, *Earthquake Eng. Struct. Dyn.* **35**, 1077–1095, available at: http://dx.doi.org/10.1002/eqe.571

Bazzurro, P., and Cornell, C. A., 1999. Disaggregation of seismic hazard, *Bull. Seismol. Soc. Am.* **89**, 501–520.

——, 2002. Vector-Valued Probabilistic Seismic Hazard Analysis (VPSHA), Paper No. 61, 1276038 (EQ)callno CF 61, *Proceedings of the 7th U.S. National Conference on Earthquake Engineering*, Boston, MA.

Bazzurro, P., and Luco, N., 2004. Parameterization of non-stationary acceleration time histories, in *Lifelines Program Project 1G00 Addenda*, Pacific Earthquake Engineering Research (PEER) Center, University of California, Berkeley, available at: http://peer.berkeley.edu/lifelines/LL-CEC/reports/final_reports/1G00-FR_pt2.pdf [accessed 10 October 2006].

Bertero, V. V., Mahin, S. A., and Herrera, R. A., 1978. Aseismic design implications of near-fault San Fernando earthquake records, *Earthquake Eng. Struct. Dyn.* **6**, 31–42.

Bray, J. D., and Rodriguez-Marek, A., 2004. Characterization of forward-directivity ground motions in the near-fault region, *Soil Dyn. Earthquake Eng.* **24**, 815–828.

Cornell, C. A., 1968. Engineering seismic risk analysis, *Bull. Seismol. Soc. Am.* **58**, 1583–1606.

Frankel, A. D., Mueller, C., Barnhard, T., Perkins, D., Leyendecker, E. V., Dickman, N., Hanson, S., and Hopper, M., 1996. *National Seismic-Hazard Maps: Documentation June 1996*, Open-File Report *96-532*, U.S. Geological Survey, available at: http://earthquake.usgs.gov/research/hazmaps/publications/hazmapsdoc/Junedoc.pdf [accessed 10 October 2006].

Fu, Q., 2005. Modeling and Prediction of Fault-Normal Near-Field Ground Motions and Structural Response, Ph.D. Dissertation, Department of Civil and Environmental Engineering, Stanford University, CA.

Fu, Q., and Menun, C., 2004. Seismic-environment-based simulation of near-fault ground motions, Paper No. 322, *Proceedings of the 13th World Conference on Earthquake Engineering*, Vancouver, BC, Canada, 1–6 August 2004.

Hall, J. F., 1998. Seismic response of steel frame buildings to near-source ground motions, *Earthquake Eng. Struct. Dyn.* **27**, 1445–1464.

Hall, J. F., and Aagaard, B. T., 1998. Fundamentals of the near-source problem, callno 630/C25/1998, *Proceedings of the 5th Caltrans Seismic Research Workshop: California Department of Transportation Engineering Service Center*, Sacramento, CA, June 16–18.

Hall, J. F., Heaton, T. H., Halling, M. W., and Wald, D. J., 1995. Near-source ground motion and its effects on flexible buildings, *Earthquake Spectra* **11**, 569–605.

Iervolino, I., and Cornell, C. A., 2007. Prediction of the occurrence of velocity pulses in near-fault ground motions, in preparation.

Iwan, W. D., 1999. Implications of near-fault ground motion for structural design, in *U.S.-Japan Workshop on Performance-Based Earthquake Engineering Methodology for Reinforced Concrete Building Structures*, PEER Report 1999/10, Maui, Hawaii, pp. 17–25.

Iwan, W. D., Huang, C.-T., and Guyader, A. C., 2000. Important features of the response of inelastic structures to near-field ground motion, Paper. No. 1740, *Proceedings of the 12th World Conference on Earthquake Engineering*, Auckland, New Zealand, January 2000.

Loh, C.-H., Wu, T.-C., and Huang, N. E., 2001. Application of the empirical mode decomposition-Hilbert spectrum method to identify near-fault ground-motion characteristics and structural responses, *Bull. Seismol. Soc. Am.* **91**, 1339–1357.

Luco, N., 2002. Probabilistic Seismic Demand Analysis, SMRF Connection Fractures, and Near-Source Effects, Ph.D. Dissertation, Department of Civil and Environmental Engineering, Stanford University, CA, available at: http://www.stanford.edu/group/rms/ [accessed 31 May 2006].

Luco, N., and Cornell, C. A., 2007. Structure-specific scalar intensity measures for near-source and ordinary earthquake ground motions, *Earthquake Spectra* **23**, 357–392.

MacRae, G. A., Morrow, D. V., and Roeder, C. W., 2001. Near-fault ground motion effects on simple structures, *J. Struct. Eng.* **127**, 996–1004.

Mavroeidis, G. P., Dong, G., and Papageorgiou, A. S., 2004. Near-fault ground motions, and the response of elastic and inelastic single-degree-of-freedom (SDOF) systems, *Earthquake Eng. Struct. Dyn.* **33**, 1023–1049.

Mavroeidis, G. P., and Papageorgiou, A. S., 2002. Near-source strong ground motion: Characteristics and design issues, *Proceedings of the 7th U.S. National Conference on Earthquake Engineering*, Boston, MA.

——, 2003. A mathematical representation of near-fault ground motions, *Bull. Seismol. Soc. Am.* **93**, 1099–1131.

McGuire, R. K., 1995. Probabilistic seismic hazard analysis and design earthquakes: Closing the loop, *Bull. Seismol. Soc. Am.* **85**, 1275–1284.

Reiter, L., 1990. *Earthquake Hazard Analysis: Issues and Insights*, Columbia University Press, New York.

Shome, N., 1999. Probabilistic Seismic Demand Analysis of Nonlinear Structures, Ph.D. Dissertation, Department of Civil and Environmental Engineering, Stanford University, CA, available at: http://www.stanford.edu/group/rms/ [accessed 10 October 2006].

Sinan, A., Ufuk, Y., and Polat, G., 2005. Drift estimates in frame buildings subjected to near-fault ground motions, *J. Struct. Eng.* **131**, 1014–1024.

Singh, J. P., 1985. Earthquake ground motions: Implications for designing structures and reconciling structural damage, *Earthquake Spectra* **1**, 239–270.

Somerville, P. G., 2003. Magnitude scaling of the near fault rupture directivity pulse, *J. Phys. Earth Planet. Interiors* **137**, 201–212.

Somerville, P. G., Smith, N., Graves, R., and Abrahamson, N., 1997. Modification of empirical strong ground motion attenuation relations to include the amplitude and duration effects of rupture directivity, *Seismol. Res. Lett.* **68**, 199–222.

Tothong, P., and Cornell, C. A., 2006a. *Probabilistic Seismic Demand Analysis Using Advanced Ground Motion Intensity Measures, Attenuation Relationships, and Near-Fault Effects*, Pacific Earthquake Engineering Research Center, *PEER Report 2006/11*, University of California, Berkeley, 2007, 205 pp.

——, 2006b. An empirical ground motion attenuation relation for inelastic spectral displacement, *Bull. Seismol. Soc. Am.* **96**, 2146–2164.

——, 2007. Structural performance assessment under near-source pulse-like ground motions using advanced ground motion intensity measures, *Earthquake Eng. Struct. Dyn.*, in review.

Tothong, P., and Luco, N., 2007. Probabilistic seismic demand analysis using advanced ground motion intensity measures, *Earthquake Eng. Struct. Dyn.* **36**, 1837–1860.

Wald, D. J., and Heaton, T. H., 1998. Forward and inverse modeling of near-source ground motions for use in engineering response analysis, Paper T162-1, *Proceedings of the American Society of Civil Engineering*, San Francisco, CA

(Received 31 January 2007; accepted 3 May 2007)